Partial Kondo screening and anomalous thermal conductance

Hee Seung Kim, Hyeok-Jun Yang, and SungBin Lee

Department of Physics, Korea Advanced Institute of Science and Technology, Daejeon 34141, Republic of Korea

The frustrated magnetism on the Kondo lattice system motivates intriguing Kondo breakdown beyond the traditional Doniach scenario. Among them, the fractionalized Fermi liquid (FL*) has drawn particular interest by virtue of its fractionalized nature. Here we study the phase diagram of the J_1-J_2 Kondo-Heisenberg model on a honeycomb lattice at a quarter filling. Employing the slave-fermion mean-field theory with $d \pm id$ spin liquid ansatz and exact diagonalization, we discuss the emergence of partial Kondo screening in the frustrated regime with comparable J_1 and J_2, and the fractionalized superconductor (SC*), which is a superconductor analogy of the FL*. Due to the larger number of local spin moments than itinerant electrons, the magnetic fluctuation is still significant even in the strong-coupling limit, which influences the thermodynamic and transport properties qualitatively. In particular, we estimate the thermal conductance to probe the low-energy excitation and show the anomalous behavior in the SC* phase in contrast to the conventional superconductors.

I. INTRODUCTION

Kondo lattice model (KLM) is prototypical for designing the heavy fermion compounds and transition-metal oxides [1–3]. After the discovery of resistivity minimum [4–6], a wealth of correlated phenomena such as the effective mass enhancement [7], quantum criticality [8–13], and unconventional superconductivity [14–17] have been reported. A great deal of theoretical interest is devoted to understanding those novel characters as a consequence of two competing tendencies, Ruderman-Kittel-Kasuya-Yosida (RKKY) interaction and the resonant hybridization on the KLM [18,19]. The underlying paradigm is that the dense arrays of magnetic impurities immersed in the metal undergo several instabilities, especially the spin-density waves and Kondo singlet formation, as the ratio of the competing energy scales varies below the Kondo temperature.

Recently, it has been spotlighted that the geometrical frustration is also decisive to the global phase diagram in Kondo physics [20–23]. In the frustrated magnet, the low-temperature paramagnet might develop a highly entangled ground state, quantum spin liquid (QSL), which turns out to be robust against small perturbations [24]. Then the Kondo coupling to the conduction electrons might lead to interesting physics, fractionalized Fermi liquid (FL*) [25,26]. Compared to conventional Fermi liquid (FL), the robustness against the Kondo screening is supported by the topological order, accompanied by the Luttinger theorem violation. An alternative possibility for the small Fermi surface is the partial Kondo screening (PKS) separated from the strong-coupling limit to some extent [27,28]. In the presence of the intermediate Kondo exchange, only a portion of local moments is hybridized, leaving the magnetic degrees of freedom. In the thermodynamic limit, it has been speculated that the portion of singlets tends to be regularly arranged on a specific sublattice.

In this way, the frustrated magnetism involves both FL* and PKS, but their collaboration on KLM leaves an open question. Starting from FL* instead of magnetic order, it is tempting to consider the coexisting characters of FL* and PKS as the Kondo coupling is turned on. If the numbers of Bloch electrons and localized $S = 1/2$ spins are stringently equal, the ground state inevitably flows to the heavy Fermi liquid in the strong-coupling limit. Then the local spin moments altogether engage in the hybridization channel. However, if there is an excess of magnetic degrees of freedom, the strongly coupled KLM does not necessarily imply the Kondo limit. Along with the electronic quasiparticles, the remaining magnetic spins still strongly fluctuate to bring about the charge-neutral spinons. As a consequence, the transport and thermodynamic behaviors are expected to exhibit both the fractionalization and hybridization characters.

In this paper we consider a J_1-J_2 Kondo-Heisenberg model on the honeycomb lattice with quarter-filled conduction electrons. Employing the ground-state ansatz of the frustrated Heisenberg model to be a $d \pm id$ spin liquid, we turn on the on-site Kondo exchange to propose the existence of a novel fractionalized phase beyond FL*. As the Kondo exchange increases, we show that only one sublattice is spontaneously hybridized, forming a Kondo resonance, while the other sublattice still retains the fractionalized excitation. Especially for a sufficiently frustrated regime where J_1 and J_2 are comparable, the proximate superconductivity is induced, preserving the chirality of the superconducting order on the itinerant side. As a consequence of existing gapless fractionalized excitation, we expect the power-law longitudinal thermal conductance behavior at the low temperature. This result is contrary to the s-wave or chiral d-wave superconductors, with the gapped spectrum exhibiting exponentially decaying behaviors. Finally, we also check that the partial Kondo screening occurs for exact diagonalization on the 18-site honeycomb lattice.
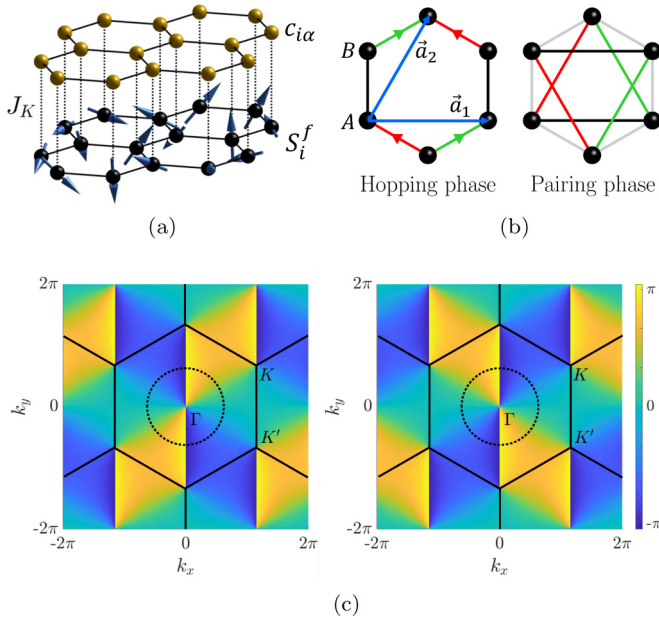
085135-1

FIG. 1. (a) Kondo-Heisenberg model on the honeycomb lattice. Upper and lower layers represent conduction electrons ($c_{i\alpha}$) and the localized moments (S_i^f) layers, respectively. Those layers are coupled by on-site Kondo coupling J_K depicted by dotted lines. (b) Nearest-neighbor hopping (left) and next-nearest-neighbor pairing (right) phases of $d \pm id$ spin liquid. Black, red, and green colors indicate 1, $e^{2\pi i/3}$, and $e^{4\pi i/3}$, respectively, and arrows on the left figure show the corresponding electron hopping direction. $\vec{a}_1$ and $\vec{a}_2$ are primitive lattice vectors, and A, B are two sublattices in the unit cell. (c) Next-nearest-neighbor pairing phase of $d \pm id$ spin liquid for the A sublattice (left) and B sublattice (right) in momentum space. Dotted line in the hexagonal plaquette shows the Fermi surface of the quarter-filled conduction electron.

II. J_1-J_2 KONDO-HEISENBERG MODEL ON THE HONEYCOMB LATTICE

In this section we study the J_1-J_2 Kondo-Heisenberg model on the quarter-filled honeycomb lattice. The system consists of two honeycomb layers [see Fig. 1(a)]. The upper layer is occupied by one itinerant electron per unit cell on average governed by the nearest-neighbor tight-binding Hamiltonian. On the other hand, the lower layer is occupied by one localized spin moment S^f with $|S^f| = 1/2$ per site governed by the nearest-neighbor and the next-nearest-neighbor antiferromagnetic Heisenberg exchanges $J_1, J_2 > 0$. Those two layers are coupled by the on-site Kondo interaction J_K whose Hamiltonian is given by

$$
\mathcal{H} = t \sum_{\langle i,j \rangle, \alpha} (c_{i\alpha}^\dagger c_{j\alpha} + \text{H.c.}) - \mu \sum_{i,\alpha} c_{i\alpha}^\dagger c_{i\alpha}
$$
$$
+ J_1 \sum_{\langle i,j \rangle} \mathbf{S}_i^f \cdot \mathbf{S}_j^f + J_2 \sum_{\langle\langle i,j \rangle\rangle} \mathbf{S}_i^f \cdot \mathbf{S}_j^f
$$
$$
+ J_K \sum_{i,\alpha\beta} \left(\frac{1}{2} c_{i\alpha}^\dagger \boldsymbol{\sigma}_{\alpha\beta} c_{i\beta} \right) \cdot \mathbf{S}_i^f, \tag{2.1}
$$

where $c_{i\alpha}^\dagger$ ($c_{i\alpha}$) is the conduction electron creation (annihilation) operator at site i on the upper layer with spin $\alpha, \beta = $

$\uparrow, \downarrow$, μ is the chemical potential for conduction electrons, and $\sigma_{\alpha\beta}$ are Pauli matrices. From now on, the conduction electron hopping parameter t is set to be unity and all energy and temperature scales are measured in units of $t = 1$.

In the decoupled limit $J_K = 0$, the upper layer is a quarter-filled metallic phase having a finite Fermi surface [dotted line in Fig. 1(c)]. The lower layer is the J_1-J_2 Heisenberg model on the honeycomb lattice whose ground state for the frustrated regime with both J_1 and J_2 is still of debate: spiral [29], plaquette valence bond solid [30], magnetically disordered [31], and spin liquid [32,33]. Among those candidates, the $d \pm id$ spin liquid ansatz, the ground state confirmed by variational Monte Carlo simulation, is of our interest to study the FL*. To proceed, we introduce a fermionic spinon operator $f_{i\alpha}$ which constitutes the localized spin operator $\mathbf{S}_i^f = f_{i\alpha}^\dagger \boldsymbol{\sigma}_{\alpha\beta} f_{i\beta}/2$. The spinon is charge neutral but carries a fractionalized quantum number spin-1/2. By employing the mean-field order parameters

$$
b_i = \langle f_{i\alpha}^\dagger c_{i\alpha} \rangle, \quad \rho_i = \varepsilon_{\alpha\beta} \langle c_{i\alpha}^\dagger f_{i\beta}^\dagger \rangle,
$$
$$
\chi_{ij} = \langle f_{i\alpha}^\dagger f_{j\alpha} \rangle, \quad \eta_{ij} = \varepsilon_{\alpha\beta} \langle f_{i\alpha}^\dagger f_{i\beta}^\dagger \rangle, \tag{2.2}
$$

the on-site Kondo Hamiltonian and localized spin-exchange terms in Eq. (2.1) for $d \pm id$ spin liquid become

$$
\mathcal{H}_K = J_K \sum_i (b_i f_i^\dagger c_i + \rho_i f_i c_i + \text{H.c.}), \tag{2.3}
$$

$$
\mathcal{H}_{J_1} = J_1 \sum_{\langle i,j \rangle \alpha} (\chi_{ij} f_{i\alpha}^\dagger f_{j\alpha} + \text{H.c.}), \tag{2.4}
$$

$$
\mathcal{H}_{J_2} = J_2 \sum_{\langle\langle i,j \rangle\rangle} (\eta_{ij} f_{i\uparrow} f_{j\downarrow} + \text{H.c.}). \tag{2.5}
$$

In Eq. (2.2), $\varepsilon_{\alpha\beta}$ is the Levi-Civita symbol, and the repeated indices are summed. The Kondo hybridization order parameters b_i and ρ_i are restricted to the on-site, while the spinon hopping $\chi_{ij} = \chi e^{i\phi_{ij}}$ and pairing $\eta_{ij} = \eta e^{i\theta_{ij}}$ run over nearest-neighbor and next-nearest-neighbor sites, respectively. Here χ and η are the self-consistently calculated real number, and ϕ_{ij} and θ_{ij} are given in Fig. 1(b). Note that the Lagrange multiplier for the spinon always vanishes $\lambda_i = 0$ to enforce the condition $\langle f_i^\dagger f_i \rangle = 1$ on average. During the mean-field calculation, we keep ϕ_{ij} and θ_{ij} for the whole range of J_1, J_2, and J_K to investigate the phase transitions out of FL*. In the next section we will explore the translation-invariant saddle-point solutions of Eq. (2.2) to Eq. (2.5).

III. MEAN-FIELD PHASE DIAGRAM

Below the critical Kondo value $0 \leqslant J_K < J_K|_c$, no electron-spinon hybridization occurs $b_i = \rho_i = 0$, which preserves the emergent gauge symmetry mediating the spinons. In this case, the mean-field solution favors different FL* phases depending on the ratio between J_1 and J_2. For $J_2/J_1 \lesssim 1$ where the frustration effect is less dominant, the spinon propagates on the uniformly finite spinon hopping order parameter strength $|\chi_{ij}| = \chi$, while the next-nearest-neighbor spinon pairing vanishes $\eta_{ij} = 0$, called the fractionalized Fermi liquid–uniform resonant valence bond phase (FL*-uRVB). The schematic order parameter configuration and corresponding spinon band structure are shown in Fig. 2(a). In the band
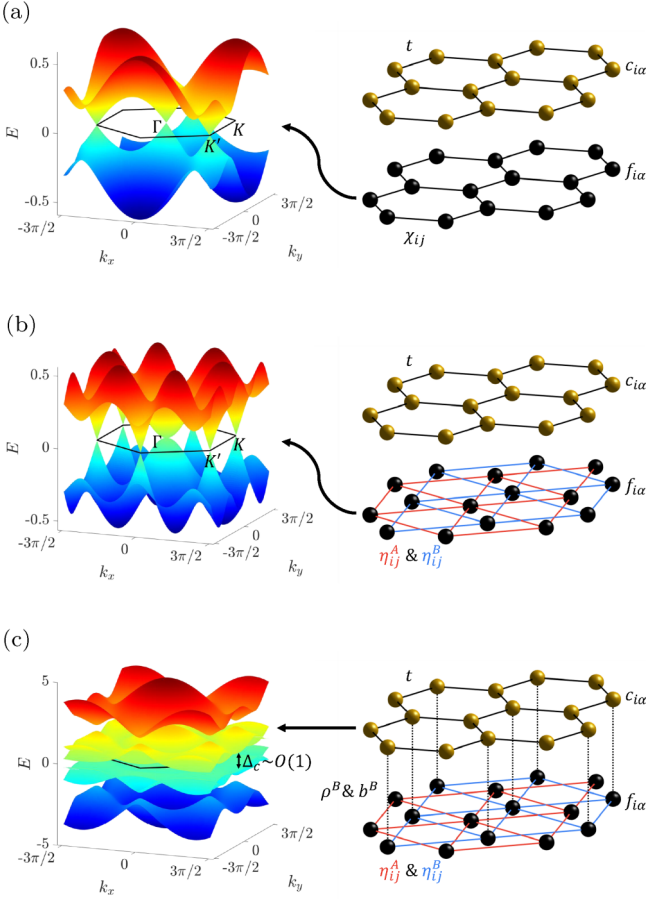
FIG. 2. The spinon band structure of (a) fractionalized Fermi liquid–uniform resonant valence bond ($J_1 = 1, J_2 = 0$) and (b) fractionalized Fermi liquid–$d \pm id$ spin liquid ($J_1 = 0, J_2 = 1$). The band structure of the $d \pm id$ spin liquid is doubly degenerate. (c) The electron band structure of a partial Kondo screening–chiral d-wave fractionalized superconductor ($J_1 = 0, J_2 = 1, J_K = 4$). The A-sublattice spinon spectrum is the same as Fig. 2(b). $\Delta_c \sim O(1)$ is the superconducting gap induced from Kondo hybridization with the B sublattice of a spinon layer. A detailed analysis about Δ_c is discussed in Sec. V. The black lines in the left column represent the first Brillouin zone boundary.

structure there are two Dirac cones at the high-symmetry points: Γ and K'. Those are protected by the product of inversion $\mathcal{P}$ and time-reversal $\mathcal{T}$ symmetries. Although the $\mathcal{PT}$-symmetric mean-field ansatz does not preserve $\mathcal{P}$ and $\mathcal{T}$ symmetry separately, the Gutzwiller projected wave function is symmetric under both $\mathcal{P}$ and $\mathcal{T}$ symmetries [32].

Increasing J_2/J_1, the first-order phase transition occurs toward the fractionalized Fermi liquid -$d \pm id$ spin liquid phase (FL*-$d \pm id$ SL) [see Fig. 2(b)]. In this case the nearest-neighbor spinon hopping order parameter vanishes, $\chi_{ij} = 0$, but has finite next-nearest-neighbor spinon pairing order parameters $\eta_{ij} \neq 0$. As shown in the right side of Fig. 2(b), two sublattices A and B on the spinon layer are completely decoupled so that the spinon spectrum in Fig. 2(b) is doubly degenerate. Even though the spinon band structure of the two sublattices are completely equivalent, the chiral structure

around the gapless points is opposite. In Fig. 1(c) we plot the phase of the next-nearest-neighbor pairing term for each sublattice on the momentum space $\eta_A(\boldsymbol{k}) = |\eta_A \boldsymbol{k}| \exp i\theta_A(\boldsymbol{k})$ and $\eta_B(\boldsymbol{k}) = |\eta_B \boldsymbol{k}| \exp i\theta_B(\boldsymbol{k})$. At the Γ point, quadratic band touching occurs and the winding number around the Γ point is $w_\Gamma = \pm 2$, or equivalently, a $d \pm id$ chiral structure, on each sublattice. In addition, there exist two Dirac cones at K and K' points with winding number $w_{K,K'} = \mp 1$, or equivalently, $p \mp ip$ chiral structure, since the winding number over the whole Brillouin zone should be 0. Those gapless points with finite chiral structure are protected by $\mathcal{PT}$ symmetry, similar to FL*-uRVB.

For sufficiently large J_K with $J_2/J_1 < 2/3$, the spinons and conduction electrons evenly take part in the hybridization ($b_i \neq 0$ and $\rho_i \neq 0$ for all i) to become a Kondo insulator (KI). As the electron-spinon hybridization order parameters b_i and ρ_i increase, the χ_{ij} and η_{ij} between hybridized sites naturally decrease, since the local spin fluctuation is suppressed rather than generating the spinon hopping or pairing.

However, if considerable frustrated Heisenberg exchange $J_1 \lesssim J_2$ exists, the one-sublattice, say B sublattice, of the honeycomb sites is spontaneously covered by the spinon-electron singlets and the other sublattice is not by virtue of the commensurate filling of conduction electrons [see Fig. 2(c)]. Therefore, $b_B, \rho_B \neq 0$, and the local moments on the A sublattice are decoupled from the Kondo singlet sites ($b_A = \rho_A = \chi_{ij} = 0$) with its own d-wave spin liquid solution optimizing Eq. (2.5) ($\eta_A \neq 0$). This quantum phenomenon is called partial Kondo screening. Although the spinon pairing is always finite on the A sublattice, the magnitude of B-sublattice pairing diminishes as the hybridization is solidified. It obviously vanishes for an infinite J_K limit, but we find a $\eta_B, b_B, \rho_B \neq 0$ solution for finite Kondo coupling strength distinct from the Kondo limit. In this case, the Cooper pairing is induced on the hybridized sites whose gap structure is inherited from $d - id$ pairing on the B-sublattice while preserving chirality. Since the A sublattice still keeps its own d-wave spin liquid induced by partial Kondo screening, the deconfined spinons coexists with the chiral d-wave superconductor, or partial Kondo screening–chiral d-wave fractionalized superconductor (PKS-dSC∗).

IV. THERMAL CONDUCTANCE BEHAVIORS

The existence of the gapless excitation and its dispersion specify the thermodynamics behaviors. The FL*-uRVB and FL*-$d \pm id$ SL contains both the electron and gapless spinon excitation. However, such excitation is frozen in the KI. The PKS-dSC∗ only contains gapless spinon excitation, and the electron sector is gapped out by electron-spinon hybridization partially inducing superconductivity. This affects the heat transport, especially the thermal conductance, which is of our interest. The thermal conductance tensor $\kappa_{\mu\nu}$ ($\mu, \nu = x, y$ in $d = 2$ spatial dimension) at temperature T is given by

$$\kappa_{\mu\nu}(T) = \frac{1}{T^2} \left(L_{\mu\nu}^{22}(T) - \frac{\left[L_{\mu\nu}^{12}(T) \right]^2}{L_{\mu\nu}^{11}(T)} \right), \qquad (4.1)$$
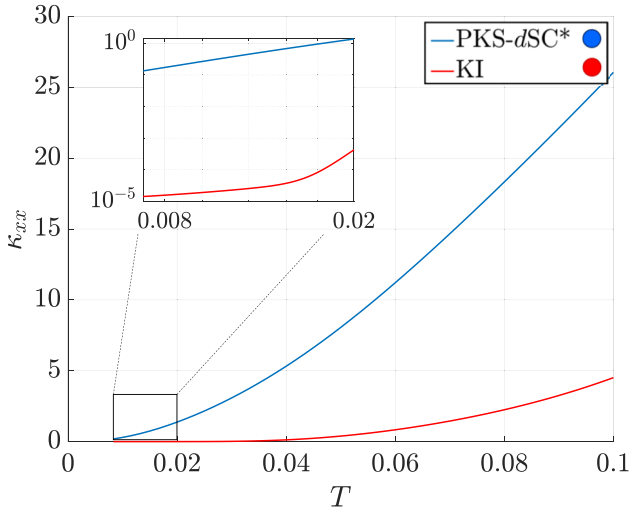
FIG. 3. Longitudinal thermal conductance-temperature plot for partial Kondo screening–chiral d-wave fractionalized superconductor (PKS-dSC∗) and Kondo insulator (KI). The inset shows a log-log plot for the low-temperature limit. The linear relation between $\log \kappa_{xx}$ and $\log T$ indicates that the low-temperature thermal conductance for PKS-dSC∗ has power-law behavior. The parameters we choose to plot are dotted blue (PKS-dSC∗) and red (KI) in Fig. 4.

where the $L_{\mu\nu}^{11}$, $L_{\mu\nu}^{12}$, and $L_{\mu\nu}^{22}$ are defined as

$$L_{\mu\nu}^{11}(T) = \int_{-\infty}^{\infty} dE[-\partial_E f(E,T)]\zeta_{\mu\nu}(E,T)$$

$$L_{\mu\nu}^{12}(T) = \int_{-\infty}^{\infty} dEE[-\partial_E f(E,T)]\zeta_{\mu\nu}(E,T)$$

$$L_{\mu\nu}^{22}(T) = \int_{-\infty}^{\infty} dEE^2[-\partial_E f(E,T)]\zeta_{\mu\nu}(E,T). \quad (4.2)$$

Here $f(E,T) = 1/(e^{\beta E} + 1)$ ($\beta = 1/T$ with $k_B = 1$) is the Fermi-Dirac distribution function, and $\zeta_{\mu\nu}(E,T)$ is

$$\zeta_{\mu\nu}(E,T) = \frac{T}{\pi N_b N_c} \sum_{b=1}^{N_b} \sum_{\boldsymbol{k}} v_{\mu}^{(b)}(\boldsymbol{k}) v_{\nu}^{(b)}(\boldsymbol{k}) [\Im G^{(b)}(\boldsymbol{k},E)]^2. \quad (4.3)$$

where $G^{(b)}(\boldsymbol{k},E)$ is a Green's function for the bth band, $v_{\mu}(\boldsymbol{k})$ is μth component of group velocity, N_b is the number of bands, and N_c is the number of grids we set in the numerical calculation.

In Fig. 3 the low-temperature behavior of longitudinal thermal conductance κ_{xx} is plotted. Blue and red lines represent the thermal conductance-temperature relation of PKS-dSC∗ and KI, which are marked as blue and red dots in Fig. 3, respectively. The inset shows a log-log plot of low temperature ($0.005 < T < 0.02$). In the KI phase, it exhibits exponential suppression due to the finite gap induced by Kondo hybridization. Meanwhile, PKS-dSC∗ features almost linear relations between the logarithm of thermal conductance and logarithm of temperature, which implies the power law of thermal conductance, even though it also has a finite gap in conduction electron layers induced by Kondo hybridization. This anomalous thermal conductance behavior comes from the gapless
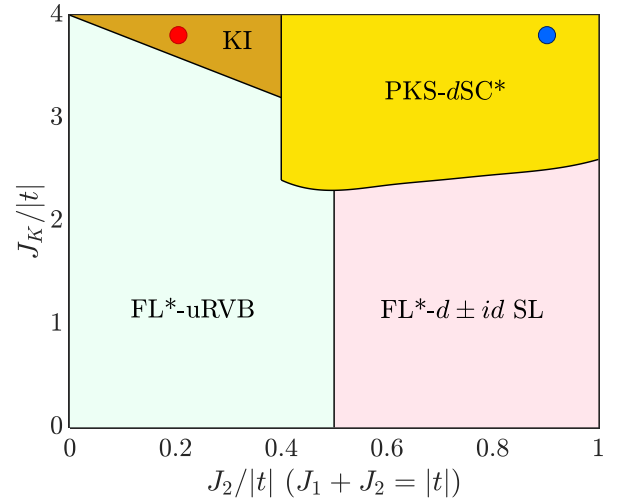

FIG. 4. The mean-field phase diagram of J_1-J_2 Kondo-Heisenberg model on the quarter-filled honeycomb lattice. Each abbreviation in the phase diagram indicates the fractionalized Fermi liquid–uniform resonant valence bond (FL*-uRVB), fractionalized Fermi liquid–$d \pm id$ spin liquid (FL*-$d \pm id$ SL), partial Kondo screening–chiral d-wave fractionalized superconductor (PKS-dSC∗), and Kondo insulator (KI). Blue and red dots are the colors for the thermal conductance plot, and add markers in Fig. 3 as well are the parameters to plot Fig. 3.

excitation of spinons which do not couple with the electron layer. Note that the thermal conductance behaviors of the conventional or gapped chiral superconductor are exponentially decaying due to their gap spectrum.

V. ANALYSIS

In the mean-field calculation, FL*-uRVB and FL*-$d \pm id$ SL are shown to be stable up to critical Kondo coupling strength (see Fig. 4). In this regime, the local spin moments strongly fluctuate but are decoupled from the itinerant electrons. The robustness of FL* compared to the conventional ordered magnet is generically guaranteed by the topological order. Here we discuss the influence of Kondo interactions on our mean-field solutions at $J_k = 0$. In the continuum $(d+1)$ dimension, the generic on-site coupling which respects the global $U(1)$ symmetry (local Z_2 symmetry) of the c (f) fermion is

$$\mathcal{S}_{\text{int}} = \sum_{\alpha\beta\gamma\delta} J_{\alpha\beta\gamma\delta} \int d^d x d\tau [c_{\alpha}^{\dagger}(\boldsymbol{x})c_{\beta}(\boldsymbol{x})][f_{\gamma}^{\dagger}(\boldsymbol{x})f_{\delta}(\boldsymbol{x})]. \quad (5.1)$$

Let us assume that the dispersion of the electron and spinon are linearized, $\varepsilon_{\boldsymbol{k}}^{c,f} \sim v^{c,f}|\boldsymbol{k}|$, on the momentum space. In the strong-coupling limit $J_{\alpha\beta\gamma\delta} \to \infty$, it obviously condensates $\langle c_{\alpha}^{\dagger}(\boldsymbol{x})f_{\beta}(\boldsymbol{x})\rangle \neq 0$ and $\langle c_{\alpha}^{\dagger}(\boldsymbol{x})f_{\beta}^{\dagger}(\boldsymbol{x})\rangle \neq 0$, which breaks the global $U(1)$ and Z_2 symmetries. In our context, this corresponds to the Kondo insulator. To examine whether the arbitrary small interaction $J_{\alpha\beta\gamma\delta}$ leads to this picture or not, we employ the dimensional analysis of Eq. (5.1). In the linearized action, the scaling dimensions of c and f fermions are $[c] = [f] = d/2$. As a result, the scaling dimension of $\mathcal{S}_{\text{int}}$ is $[J_{\alpha\beta\gamma\delta}] = 1 - d$, which implies the irrelevance of Eq. (5.1)

for spatial dimensions larger than 1 at the tree level. If the local spin operators are fractionalized into deconfined spinons, the power counting is applicable to the Kondo interaction in Eq. (5.2). This argument supports the reliability of our mean-field results in Fig. 4 and clarifies the Kondo breakdown for small J_K separated from the heavy Fermi liquid.

We now discuss the chiral gap structure on the itinerant electrons induced by partial Kondo screening. With the itinerant electron side, the mean-field decoupled Hamiltonian equations (2.3) to (2.5) can be arranged as

$$\mathcal{H} = \sum_{\boldsymbol{k}} \begin{pmatrix} \Psi_c(\boldsymbol{k}) \\ \Psi_f(\boldsymbol{k}) \end{pmatrix}^{\dagger} \begin{pmatrix} H_c(\boldsymbol{k}) & K \\ K^{\dagger} & H_f(\boldsymbol{k}) \end{pmatrix} \begin{pmatrix} \Psi_c(\boldsymbol{k}) \\ \Psi_f(\boldsymbol{k}) \end{pmatrix}, \quad (5.2)$$

$$\Psi_{c,f}(\boldsymbol{k}) = \begin{pmatrix} c, f_{A\uparrow}(\boldsymbol{k}) \\ c, f_{A\downarrow}^{\dagger}(-\boldsymbol{k}) \\ c, f_{B\uparrow}(\boldsymbol{k}) \\ c, f_{B\downarrow}^{\dagger}(-\boldsymbol{k}) \end{pmatrix} \equiv \begin{pmatrix} \psi_{c,f}^{\mathrm{U}}(\boldsymbol{k}) \\ \psi_{c,f}^{\mathrm{S}}(\boldsymbol{k}) \end{pmatrix}, \quad (5.3)$$

where $H_c(\boldsymbol{k})$ and $H_f(\boldsymbol{k})$ are the electron and spinon Hamiltonian matrix at $\boldsymbol{k}$, respectively. $H_c(\boldsymbol{k})$ and $H_f(\boldsymbol{k})$ are connected via the translation-invariant on-site Kondo coupling matrix K and are thus momentum independent. Beyond the critical Kondo coupling strength with a frustrated regime, we know that one sublattice spontaneously hybridizes with electron layers. Let us assume that the hybridized sublattice is a B sublattice [see Fig. 2(c)]. Then we can divide the A and B sublattice as Kondo unscreened and screened sites, denoted as U and S in the superscript. From now on we omit the momentum dependency of the Hamiltonian matrices and basis operators unless there is any confusion.

When $J_K \geqslant J_K^c$, the Kondo coupling matrix K and spinon Hamiltonian H_f become

$$\Psi_c^{\dagger} K \Psi_f = \begin{pmatrix} \psi_c^{\mathrm{U}} \\ \psi_c^{\mathrm{S}} \end{pmatrix}^{\dagger} \begin{pmatrix} \boldsymbol{K}^{\mathrm{U}} = \boldsymbol{0} & \boldsymbol{0} \\ \boldsymbol{0} & \boldsymbol{K}^{\mathrm{S}} \end{pmatrix} \begin{pmatrix} \psi_f^{\mathrm{U}} \\ \psi_f^{\mathrm{S}} \end{pmatrix}, \quad (5.4)$$

$$\Psi_f^{\dagger} H_f \Psi_f = \begin{pmatrix} \psi_f^{\mathrm{U}} \\ \psi_f^{\mathrm{S}} \end{pmatrix}^{\dagger} \begin{pmatrix} \boldsymbol{H}_f^{\mathrm{U}} & \boldsymbol{h}_f = \boldsymbol{0} \\ \boldsymbol{h}_f^{\dagger} = \boldsymbol{0} & \boldsymbol{H}_f^{\mathrm{S}} \end{pmatrix} \begin{pmatrix} \psi_f^{\mathrm{U}} \\ \psi_f^{\mathrm{S}} \end{pmatrix}, \quad (5.5)$$

where $\boldsymbol{K}^{\mathrm{S}}$ is a nonzero matrix that hybridizes the electron and spinon on the Kondo screened sites. We note that the Kondo matrix for the unscreened sites is $\boldsymbol{K}^{\mathrm{U}} = \boldsymbol{0}$, as the name unscreened depicts. As we discussed earlier, finite order parameters for Kondo coupling on the Kondo screened sites implies that the spinon on the Kondo screened sites prefers interacting with electrons rather than spinons. Thus we have $\boldsymbol{h}_f = \boldsymbol{0}$, making spinons on the Kondo unscreened sites completely decoupled to the electron layer and spinons on the Kondo screened sites.

Let us first calculate the induced electron Hamiltonian driven by PKS. We integrate out Eq. (5.5) from Eq. (5.2) and obtain the effective electron action $\mathcal{S}_c^{\mathrm{eff}}$, given as

$$\mathcal{S}_c^{\mathrm{eff}} = \sum_{\boldsymbol{k}, i\omega_n} \bar{\Psi}_c \big(G_c^{-1} - K G_f K^{\dagger} \big) \Psi_c, \quad (5.6)$$

where $G_{c,f} = (-i\omega_n + H_{c,f})^{-1}$ is the Green's function of the electron and spinon, and $\omega_n = (2n+1)\pi/\beta$ is the fermionic Matsubara frequency. At low temperature, the induced term of Eq. (5.6) can be outlined by substituting $\omega_n = 0$ as

$$\Psi_c^{\dagger} K \tilde{G}_f K^{\dagger} \Psi_c = \begin{pmatrix} \psi_c^{\mathrm{U}} \\ \psi_c^{\mathrm{S}} \end{pmatrix}^{\dagger} \begin{pmatrix} \boldsymbol{0} & \boldsymbol{0} \\ \boldsymbol{0} & \boldsymbol{K}^{\mathrm{S}}[\boldsymbol{H}_f^{\mathrm{S}}]^{-1}\boldsymbol{K}^{\mathrm{S}\dagger} \end{pmatrix} \begin{pmatrix} \psi_c^{\mathrm{S}} \\ \psi_c^{\mathrm{U}} \end{pmatrix}. \quad (5.7)$$

Let us assume that the Kondo screened sites form a translation-invariant lattice structure with a single sublattice, such as a triangular or square lattice. Then $\boldsymbol{H}_f^{\mathrm{S}}$ and $\boldsymbol{K}^{\mathrm{S}}$ can be written in 2×2 matrix form in the momentum space as

$$\psi_c^{\mathrm{S}\dagger} \boldsymbol{K}^{\mathrm{S}} \psi_f^{\mathrm{S}} = (c_{\boldsymbol{k}\uparrow}^{\dagger} \quad c_{-\boldsymbol{k}\downarrow}) \begin{pmatrix} b & \rho^* \\ \rho & -b^* \end{pmatrix} \begin{pmatrix} f_{\boldsymbol{k}\uparrow} \\ f_{-\boldsymbol{k}\downarrow}^{\dagger} \end{pmatrix},$$

$$\psi_f^{\mathrm{S}\dagger} \boldsymbol{H}_f^{\mathrm{S}} \psi_f^{\mathrm{S}} = (f_{\boldsymbol{k}\uparrow}^{\dagger} \quad f_{-\boldsymbol{k}\downarrow}) \begin{pmatrix} \xi_f & \eta^* \\ \eta & -\xi_f \end{pmatrix} \begin{pmatrix} f_{\boldsymbol{k}\uparrow} \\ f_{-\boldsymbol{k}\downarrow}^{\dagger} \end{pmatrix}, \quad (5.8)$$

where b, ρ, and η are defined in Eq. (2.2). Inserting Eq. (5.8) into Eq. (5.7), the induced electron Hamiltonian on the Kondo screened sites near the Fermi surface becomes

$$\boldsymbol{H}_c^{\mathrm{S}} \equiv -\boldsymbol{K}^{\mathrm{S}}[\boldsymbol{H}_f^{\mathrm{S}}]^{-1}\boldsymbol{K}^{\mathrm{S}\dagger} \equiv \begin{pmatrix} \xi_c^{\mathrm{S}} & \Delta_c^{\mathrm{S}*} \\ \Delta_c^{\mathrm{S}} & -\xi_c^{\mathrm{S}} \end{pmatrix} = \frac{1}{\xi_f^2 + |\eta|^2} \begin{pmatrix} -2\Re[\eta^* b\rho] - \xi_f(|b|^2 - |\rho|^2) & b^2\eta^* - \rho^{*2}\eta - 2b\rho^*\xi_f \\ b^{*2}\eta - \rho^2\eta^* - 2b^*\rho\xi_f & 2\Re[\eta^* b\rho] + \xi_f(|b|^2 - |\rho|^2) \end{pmatrix}, \quad (5.9)$$

where $\Re$ is the real part, and ξ_c^{S} and Δ_c^{S} are induced electron hopping and the pairing term on the Kondo screened sites.

Close to the Fermi surface where the denominator is non-vanishing, we focus on the induced Cooper pairing in the itinerant electron layer. In our saddle-point solutions, it turns out that $|\rho| < |b|$ and thus the off-diagonal Δ_c^{S} is largely contributed from $b^{*2}\eta$. Therefore, the chirality of induced electron pairing has the same chiral structure of spinons on the hybridized sublattice. Furthermore, the magnitudes of order parameters in our numerical solution are given as $\xi_f =$

0, $|b| \sim O(10^{-1})$, $|\eta| \sim O(10^{-2})$, and $|\rho| \sim O(10^{-3})$ and result in $|\xi_c^{\mathrm{S}}| \sim O(10^{-2})$ and $|\Delta_c^{\mathrm{S}}| \sim O(1)$, which implies that the superconducting gap has an order of 1. In Fig. 2(c), $\Delta_c \sim O(1)$, which perfectly matches with our analytical calculation.

VI. CONCLUSIONS

In this work we study the J_1-J_2 Kondo-Heisenberg model at quarter-filled conduction electrons on the honeycomb

lattice. Based on the slave-fermion mean-field approach, a new fractionalized phase, called a PKS-dSC∗ phase, out of the weak-coupling FL* regime is proposed by turning on the Kondo coupling collaborated with frustrated RKKY exchanges. This phase appears for a wide range of mean-field phase diagrams having a fractionalized spinon excitation due to the frustration effect endowed with the unbalanced filling. We then discuss the stability of fractional excitation against the Kondo exchange, the chirality of the induced superconductivity, and the thermal conductance behaviors for each phase as the temperature varies.

For sufficiently large $J_K \gg J_1, J_2$, we check that the partial Kondo screening occurs when $J_2/J_1 \gtrsim 2$ by exact diagonalization up to 18 sites in the honeycomb lattice with open-boundary conditions (see Appendix A for details). Therefore it will be interesting to study the partial Kondo screening out of FL* beyond the mean-field regime on the different frustrated lattice systems. Furthermore, we can also consider the Lifshitz transition controlled by the filling factor. As can be seen in Fig. 1(c), there is a $p \mp ip$ pairing structure around the K and K' points for FL*-$d \pm id$ SL. Therefore if the electron filling factor becomes larger than $1/3$ and thus the Fermi surface surrounds the K and K' points, keeping partial Kondo screening, we expect the Lifshitz transition from PKS-dSC∗ to PKS-pSC∗, which will be left for future work.

APPENDIX: EXACT DIAGONALIZATION

First of all, we have solved the J_1-J_2 Kondo-Heisenberg model with three electrons by exact diagonalization for a small system size ($N = 6$ sites with a hexagonal shape). In this case, the Kondo singlet pair only exists on the one sublattice, and the others do not for frustration limit ($J_2 \geqslant J_1$) with sufficient Kondo coupling strength. Based on this result, we have considered an $N = 18$ site ($2 \times 3 \times 3$ open-boundary condition) honeycomb lattice in the following way. In the procedure we first consider the half of sites already formed by the Kondo singlet pairing between localized spins and quarter-filled electrons. Then we compute the exact ground state and corresponding energy for the J_1-J_2 Heisenberg model on the remaining sites and focus on the lowest energy states. We find out that the lowest energy state prefers Kondo singlet pairing only on the one sublattice.

[1] G. R. Stewart, Rev. Mod. Phys. **56**, 755 (1984).

[2] A. C. Hewson, *The Kondo Problem to Heavy Fermions*, Cambridge Studies in Magnetism (Cambridge University Press, Cambridge, England, 1993).

[3] H. v. Löhneysen, A. Rosch, M. Vojta, and P. Wölfle, Rev. Mod. Phys. **79**, 1015 (2007).

[4] W. de Haas, J. de Boer, and G. van deën Berg, Physica **1**, 1115 (1934).

[5] J. Kondo, Prog. Theor. Phys. **32**, 37 (1964).

[6] M. D. Daybell and W. A. Steyert, Rev. Mod. Phys. **40**, 380 (1968).

[7] K. Andres, J. E. Graebner, and H. R. Ott, Phys. Rev. Lett. **35**, 1779 (1975).

[8] M. B. Maple, C. L. Seaman, D. A. Gajewski, Y. Dalichaouch, V. B. Barbetta, M. C. de Andrade, H. A. Mook, H. G. Lukefahr, O. O. Bernal, and D. E. MacLaughlin, J. Low Temp. Phys. **95**, 225 (1994).

[9] P. Coleman, C. Pépin, Q. Si, and R. Ramazashvili, J. Phys.: Condens. Matter **13**, R723 (2001).

[10] P. Gegenwart, J. Custers, C. Geibel, K. Neumaier, T. Tayama, K. Tenya, O. Trovarelli, and F. Steglich, Phys. Rev. Lett. **89**, 056402 (2002).

[11] S. Paschen, T. Lühmann, S. Wirth, P. Gegenwart, O. Trovarelli, C. Geibel, F. Steglich, P. Coleman, and Q. Si, Nature (London) **432**, 881 (2004).

[12] G. R. Stewart, Rev. Mod. Phys. **78**, 743 (2006).

[13] P. Gegenwart, Q. Si, and F. Steglich, Nat. Phys. **4**, 186 (2008).

[14] N. D. Mathur, F. M. Grosche, S. R. Julian, I. R. Walker, D. M. Freye, R. K. W. Haselwimmer, and G. G. Lonzarich, Nature (London) **394**, 39 (1998).

[15] C. Pfleiderer, Rev. Mod. Phys. **81**, 1551 (2009).

[16] F. Steglich, J. Phys.: Conf. Ser. **400**, 022111 (2012).

[17] O. Bodensiek, R. Žitko, M. Vojta, M. Jarrell, and T. Pruschke, Phys. Rev. Lett. **110**, 146406 (2013).

[18] C. M. Varma, Rev. Mod. Phys. **48**, 219 (1976).

[19] S. Doniach, Physica B+C **91**, 231 (1977).

[20] S. Burdin, D. R. Grempel, and A. Georges, Phys. Rev. B **66**, 045111 (2002).

[21] T. T. Ong and B. A. Jones, Phys. Rev. Lett. **103**, 066405 (2009).

[22] P. Coleman and A. H. Nevidomskyy, J. Low Temp. Phys. **161**, 182 (2010).

[23] Q. Si and S. Paschen, Phys. Status Solidi B **250**, 417 (2013).

[24] L. Savary and L. Balents, Rep. Prog. Phys. **80**, 016502 (2017).

[25] T. Senthil, S. Sachdev, and M. Vojta, Phys. Rev. Lett. **90**, 216403 (2003).

[26] T. Senthil, M. Vojta, and S. Sachdev, Phys. Rev. B **69**, 035111 (2004).

[27] Y. Motome, K. Nakamikawa, Y. Yamaji, and M. Udagawa, Phys. Rev. Lett. **105**, 036403 (2010).

[28] T. Sato, F. F. Assaad, and T. Grover, Phys. Rev. Lett. **120**, 107201 (2018).

[29] J. Oitmaa and R. R. P. Singh, Phys. Rev. B **84**, 094424 (2011).

[30] S.-S. Gong, D. N. Sheng, O. I. Motrunich, and M. P. A. Fisher, Phys. Rev. B **88**, 165138 (2013).

[31] F. Mezzacapo and M. Boninsegni, Phys. Rev. B **85**, 060402(R) (2012).

[32] F. Ferrari, S. Bieri, and F. Becca, Phys. Rev. B **96**, 104401 (2017).

[33] B. K. Clark, D. A. Abanin, and S. L. Sondhi, Phys. Rev. Lett. **107**, 087204 (2011).